Xiaowei Deng
Department of Structural Engineering,
University of California, San Diego,
La Jolla, CA 92093
e-mail: x8deng@eng.ucsd.edu

Yingjun Wang[1]
Department of Structural Engineering,
University of California, San Diego,
La Jolla, CA 92093
e-mail: yiw009@eng.ucsd.edu

Jinhui Yan
Department of Structural Engineering,
University of California, San Diego,
La Jolla, CA 92093
e-mail: jiy071@eng.ucsd.edu

Tao Liu
Wuhan Heavy Duty Machine Tool,
Group Co., Ltd.,
Wuhan 430205, China
e-mail: tower.lau@qq.com

Shuting Wang
Professor
School of Mechanical Science and Engineering,
Huazhong University of Science and Technology,
Wuhan 430074, China
e-mail: wangst@mail.hust.edu.cn

Topology Optimization of Total Femur Structure: Application of Parameterized Level Set Method Under Geometric Constraints

Optimization of the femur prosthesis is a key issue in femur replacement surgeries that provide a viable option for limb salvage rather than amputation. To overcome the drawback of the conventional techniques that do not support topology optimization of the prosthesis design, a parameterized level set method (LSM) topology optimization with arbitrary geometric constraints is presented. A predefined narrow band along the complex profile of the original femur is preserved by applying the contour method to construct the level set function, while the topology optimization is carried out inside the cavity. The Boolean R-function is adopted to combine the free boundary and geometric constraint level set functions to describe the composite level set function of the design domain. Based on the minimum compliance goal, three different designs of 2D femur prostheses subject to the target cavity fill ratios 34%, 54%, and 74%, respectively, are illustrated.
[DOI: 10.1115/1.4031803]

1 Introduction

Proximal and total femur resections with endoprosthetic reconstruction are complex surgical procedures because of their safety and good functional outcome [1]. Figure 1 highlights the satisfactory appearance of a femur radiograph 14 months after a femur replacement surgery. However, the femur replacement with a modular prosthesis can be risky in the long term because it may cause stress shielding, which refers to the development of osteoporosis or resorption of the cortical bone as a result of removal of stress from the bone by an implant [3,4]. Khanoki and Pasini designed a novel hip implant made of a cellular material having a periodic micro-architecture, i.e., a lattice displaying graded property distribution to avoid progressive damage and fatigue caused by daily cyclic loading [5–7]. In this approach, a multi-objective optimization strategy based on minimization of two conflicting indices, bone resorption and interface stress, is combined with multiscale analysis of the hip implant with controlled lattice micro-architecture.

The idea of the prosthetic design is to adopt the external shape of the original femur by preserving certain thickness along the profile for effective muscle and tendon reattachment. A contact surface similar to the original condition results in even distribution of stress transmitted to the articular cartilage and the subchondral bone, and thereby reduces the risk of wear and erosion [8]. Wolf's law assumes that the bone is capable of adapting to the mechanical stimulation and optimizing energy expenditure to keep the tissue in a good condition [9]. Bone adaption can be

Fig. 1 Fourteen months postoperative radiograph of a 73-year-old man after total femur replacement [2]

[1]Corresponding author.

Contributed by the Design Automation Committee of ASME for publication in the Journal of Mechanical Design. Manuscript received December 14, 2014; final manuscript received September 22, 2015; published online November 16, 2015. Assoc. Editor: James K. Guest.

considered as the optimization problem of minimizing the total bone strain energy corresponding to the given loading condition [10]. Therefore, in this paper, topology optimization aims at the objective of minimal strain energy of the total femur subject to the designated total weight and is performed inside the cavity domain [11,12].

Topology optimization has become a powerful and effective tool to improve the mechanical designs [13,14]. The earliest research of topology optimization in engineering can be traced back to the well-known "Michell truss" that is a plane truss with an optimal stiffness for a given weight in 1904 [15]. Researchers have made a significant progress since the homogenization method [16], the solid isotropic microstructure with penalization method [17], and the evolutionary structural optimization [18] were proposed. The above methods, which adopt explicit material representation [19–21], are element-based optimization methods, and thus their results are usually identified with zigzag features [22,23].

This deficiency can be overcome by the level-set-based topology optimization method which adopts an implicit description of boundaries. The LSM was proposed by Osher and Sethian [24] who used level sets as a tool to track and model the evolution of moving boundaries. The LSM was first applied to topology optimization in the early 2000s by Sethian and Wiegmann [25] to capture the free boundary of a structure. Osher and Santosa [26] combined LSM with a shape sensitivity analysis framework for structural optimization in 2001. Wang et al. [22,27] proposed a "velocity vector" to setup the Hamilton–Jacobi partial differential equation (PDE), which naturally related to the shape derivative from the classical shape variational analysis. Another branch of the LSM was developed by Allaire et al. [28–30], who independently developed a numerical framework that used the velocity of level set boundaries for shape sensitivity analysis. A predictor–corrector scheme for constructing the velocity field in level-set-based topology optimization was developed to improve the computational efficiency [31]. Zhu et al. [32] proposed a two-step elastic modeling method for the topology optimization of compliant mechanisms aimed at eliminating de facto hinges and a high efficiency optimization algorithm that can yield fewer design iterations.

For conventional LSMs, the Hamilton–Jacobi PDE was solved explicitly, which decreased the efficiency because of the limitation of the time step size for convergence stability and reinitialization of level set functions. In contrast, the parameterized LSM converted the Hamilton–Jacobi PDE into a simpler set of ordinary differential equations using radial basis functions (RBFs) [33,34]. Luo et al. [35–37] further presented a parameterized LSM using compactly supported RBFs (CSRBFs). Wei et al. [38] introduced the extended finite element method (XFEM) into RBF-based level-set structural optimization to address the elements across the boundaries and obtained more accurate optimal results.

Geometric shape control plays an important role in the topology optimization problem. Some researchers have made pioneering contributions in this field. Chen et al. [39,40] used the R-function in a B-spline parameterized level set topology optimization to realize the explicit parametric control of geometry and topology within a large space of free form shapes. Chen et al. [41] employed high-order energy functional in the topology optimization to generate striplike designs with a specified feature width. Recently, Guo et al. [42] proposed a scheme for complete explicit control of the feature sizes in topology optimization using the signed distance function. Allaire et al. [43] proposed a thickness control based on the signed distance function. Liu et al. [44,45] used the parameterized LSM with the CSRBF and R-function for a unified topology and shape optimization method of a continuum structure with geometric constrains, and later applied them to eigenvalue topology optimization.

The geometric constraints imposed by the R-functions are efficient in solving simple geometry problems, but they may become computationally expensive to setup the level set functions for the complex geometries. Detailed explanations are presented in Sec. 2.2.1 with an example. Therefore, we perform topology optimization of a 2D femur structure by developing new techniques that combines contour functions and Boolean operations to configure the level set functions. Note that material optimization or multiscale design based on homogenization of microstructures are beyond the scope of the paper [7,46]. Only one isotropic material, e.g., titanium alloy, is used in the optimization.

2 Methods

In this paper, the objective of topology optimization is to minimize compliance of the design subject to the goal weight, which is performed based on the framework of CS-RBF parameterized LSM [44]. In the context of implicit geometric representation, the structural boundary is defined as the zero level set, and the evolution of the level set function is governed by the Hamilton–Jacobi PDE. As an extension of the traditional level set scheme, the contour function satisfying Lipschitz continuity is specially chosen to build the level-set function of the irregular femur profile as geometric constraints. The shape derivative method is implemented to find the sensitivities of the objective function and constraint with respect to the expansion coefficients of the basis functions, while XFEM is used to compute the stiffness matrix and the optimality criteria method used to solve the optimization problem.

2.1 Parameterized LSM. Figure 2 gives an example of a 2D design domain Ω with level set function. The design boundary $\partial\Omega$ is implicitly embedded as the zero level set of a level set function $\Phi(\mathbf{x}, t)$, where t is a pseudotime. The $\Phi(\mathbf{x}, t)$ can be defined over a reference domain $D \subset R^d$ ($d = 2$ or 3) including all the admissible shapes. The scheme of the 2D structure can be defined as

$$\begin{cases} \Phi(\mathbf{x},t) > 0 \Longleftrightarrow \mathbf{x} \in \Omega \backslash \partial\Omega \ \text{ at time } \ t & (\text{inside the boundary}) \\ \Phi(\mathbf{x},t) = 0 \Longleftrightarrow \mathbf{x} \in \partial\Omega \cap D \ \text{ at time } \ t & (\text{on the boundary}) \\ \Phi(\mathbf{x},t) < 0 \Longleftrightarrow \mathbf{x} \in D \backslash \Omega \ \text{ at time } \ t & (\text{outside the boundary}) \end{cases} \tag{1}$$

The Hamilton–Jacobi equation is obtained by taking the derivative of the level set function $\Phi(\mathbf{x}, t)$ with respect to the pseudotime t [27,37]

$$\frac{\partial \Phi(\mathbf{x},t)}{\partial t} - \nu_n |\nabla \Phi| = 0, \quad \Phi(\mathbf{x},0) = \Phi_0(\mathbf{x}) \tag{2}$$

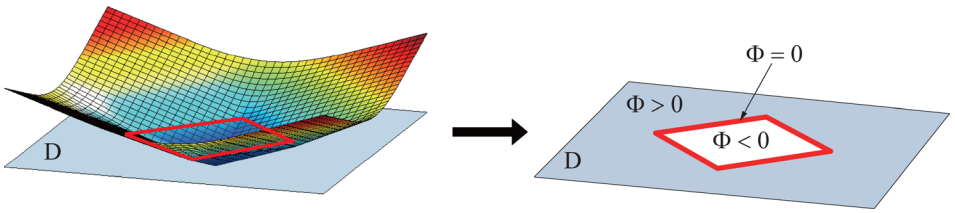

Fig. 2 A 2D design domain and the level set model

where the normal velocity $\nu_n = \nu \cdot (\nabla\Phi/|\nabla|\Phi)$, and $\Phi_0(\mathbf{x})$ is the initial level set function.

The scalar level set function can be interpolated at the knots as

$$\Phi(\mathbf{x}, t) = \varphi(\mathbf{x})^{\mathrm{T}}\alpha(t) = \sum_{i=1}^{n} \phi_i(\mathbf{x})\alpha_i(t) \tag{3}$$

where n is the number of knots, $\varphi(\mathbf{x}) = [\phi_1(\mathbf{x}), \phi_2(\mathbf{x}), \ldots, \phi_n(\mathbf{x})]^{\mathrm{T}}$ is the interpolation vector of the shape functions, and $\alpha(t) = [\alpha_1(t), \alpha_2(t), \ldots, \alpha_n(t)]^{\mathrm{T}}$ is the expansion coefficient vector. Note that for parametric LSM, updating of the level set function during each optimization iteration is directly operated based on the expansion coefficients. A CS-RBF with C_2 smoothness, because of a strictly positive definiteness and sparsity of collection matrices [47,48], is adopted to interpolate the level set function as follows [35]:

$$\phi(r) = [\max(0, (1-r)^4)] \cdot (4r+1) \tag{4}$$

where the radius of support r is the scaling distance from knot (x, y) to knot (x_i, y_i)

$$r = \frac{\sqrt{(x-x_i)^2 + (y-y_i)^2}}{d} \tag{5}$$

where d is a scaling parameter factor chosen 2–4 times of the element size [36]. By substituting Eq. (3) to Eq. (2), the space and time of the Hamilton–Jacobi PDE are separated and the PDE can be rewritten as

$$\varphi(\mathbf{x})^{\mathrm{T}}\frac{d\alpha(t)}{dt} - \nu_n|(\nabla\varphi)^{\mathrm{T}}\alpha(t)| = 0 \tag{6}$$

where ν_n related to the time derivative of the expansion coefficients is expressed as

$$\nu_n = \frac{\varphi(\mathbf{x})^{\mathrm{T}}}{|(\nabla\varphi)^{\mathrm{T}}\alpha(t)|}\frac{d\alpha(t)}{dt} \tag{7}$$

In this way, the original level set optimization problem is converted into a parameterized level set optimization problem.

2.2 Level Set Model Including Arbitrary Geometric Constraint. In this section, contour function method based on the minimal point-polygon distance is proposed to construct a level set function for topology optimization with complex geometric constraints, e.g., concave profile of a total femur.

2.2.1 Conventional Level Set Function for Regular Convex Geometries. For a simple convex geometry, e.g., a circle, the level set function can be directly derived from the circle equation as

$$\Phi_c(x, y) = r_c^2 - (x-x_0)^2 - (y-y_0)^2 \tag{8}$$

where (x, y) is a point in the design domain, r_c is the radius of the circle, and (x_0, y_0) is the center of the circle.

A general Boolean operation can represent a complex geometry on multiple simple geometries. Similarly, the level set function of design domain is obtained by a large number of Boolean operations $\cap$ and $\cup$ through the R-functions. One pair of R-functions can be written as follows:

$$\Phi_1 \cap \Phi_2 = \frac{1}{1+a}\left(\Phi_1 + \Phi_2 - \sqrt{\Phi_1^2 + \Phi_2^2 - 2a\Phi_1\Phi_2}\right) \tag{9}$$

$$\Phi_1 \cup \Phi_2 = \frac{1}{1+a}\left(\Phi_1 + \Phi_2 + \sqrt{\Phi_1^2 + \Phi_2^2 - 2a\Phi_1\Phi_2}\right) \tag{10}$$

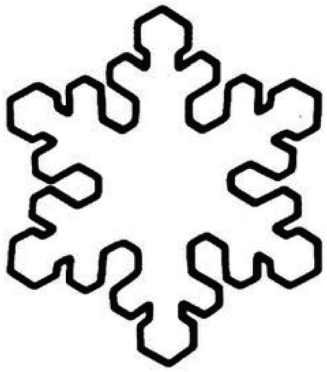

Fig. 3 Example of complex geometry: snowflake pattern

where a is an arbitrary parameter that satisfies $|a| \leq 1$. Parametric study showed that $a = 0.5$, as adopted in the paper, performed the best to balance both the convergence speed and the smoothness of design boundary at the same time [44]. Therefore, a more general method to construct the level set function of a convex polygon is using R-function to combine boundary line functions, e.g., the level set functions of three edges of a triangle are

$$\begin{cases} \Phi_1(x, y) = a_1x + b_1y + c_1 \\ \Phi_2(x, y) = a_2x + b_2y + c_2 \\ \Phi_3(x, y) = a_3x + b_3y + c_3 \end{cases} \tag{11}$$

where a_i, b_i, c_i $(i = 1, 2, 3)$ are coefficients, and then the level set function of the triangle is constructed by R-function as

$$\Phi_R(x, y) = \Phi_1(x, y) \cap \Phi_2(x, y) \cap \Phi_3(x, y) \tag{12}$$

A major disadvantage of the above method is that it may be costly for the complex nonconcave geometries, as shown in Fig. 3. It limits the application of level set topology optimization to the artificial femur prosthesis because of the complexity of its geometric profile that should match the curve of the neighboring articular cartilage.

2.2.2 Contour Function for Arbitrary Geometric Constraint. In order to realize the level set topology optimization with geometric constraints, we will propose contour function method to construct a level set function of arbitrary geometry $\Phi_R(\mathbf{x}_i)$. For a 2D problem, since the enclosed boundary curve can be approximated as a polygon, in contour function, the amplitude is determined by the minimal point-polygon distance and its sign is determined by the position relation of point and polygon. Apparently, for any point on the polygon, the minimal point and boundary line distance is zero, which represents zero level set. The point-in-polygon (PIP) problem is a typical problem in computational geometry that asks whether a given point in the plane lies inside, outside, or on the boundary of a polygon. One simple solution of PIP problem is ray casting algorithm or also known as crossing number algorithm [49,50]. It first tests how many times a ray, starting from the point and going in any fixed direction, intersects the edges of the polygon. In the case that the given point is not on the boundary of the polygon, it is outside if the number of intersections is an even number, and it is inside if odd. The procedure of construction contour function is shown as follows:

- Step 1: Extract the enclosed boundary line Γ of the model and discretize the line into m segments along the counterclockwise direction. Note that a curved boundary line should be partitioned to more segments for higher accuracy.
- Step 2: For an arbitrary knot i inside or outside the boundary line Γ, loop over all the segments and compute the minimal distance d_{ij} $(j = 1, 2, \ldots m)$ between the knot i and each segment j with finite length.

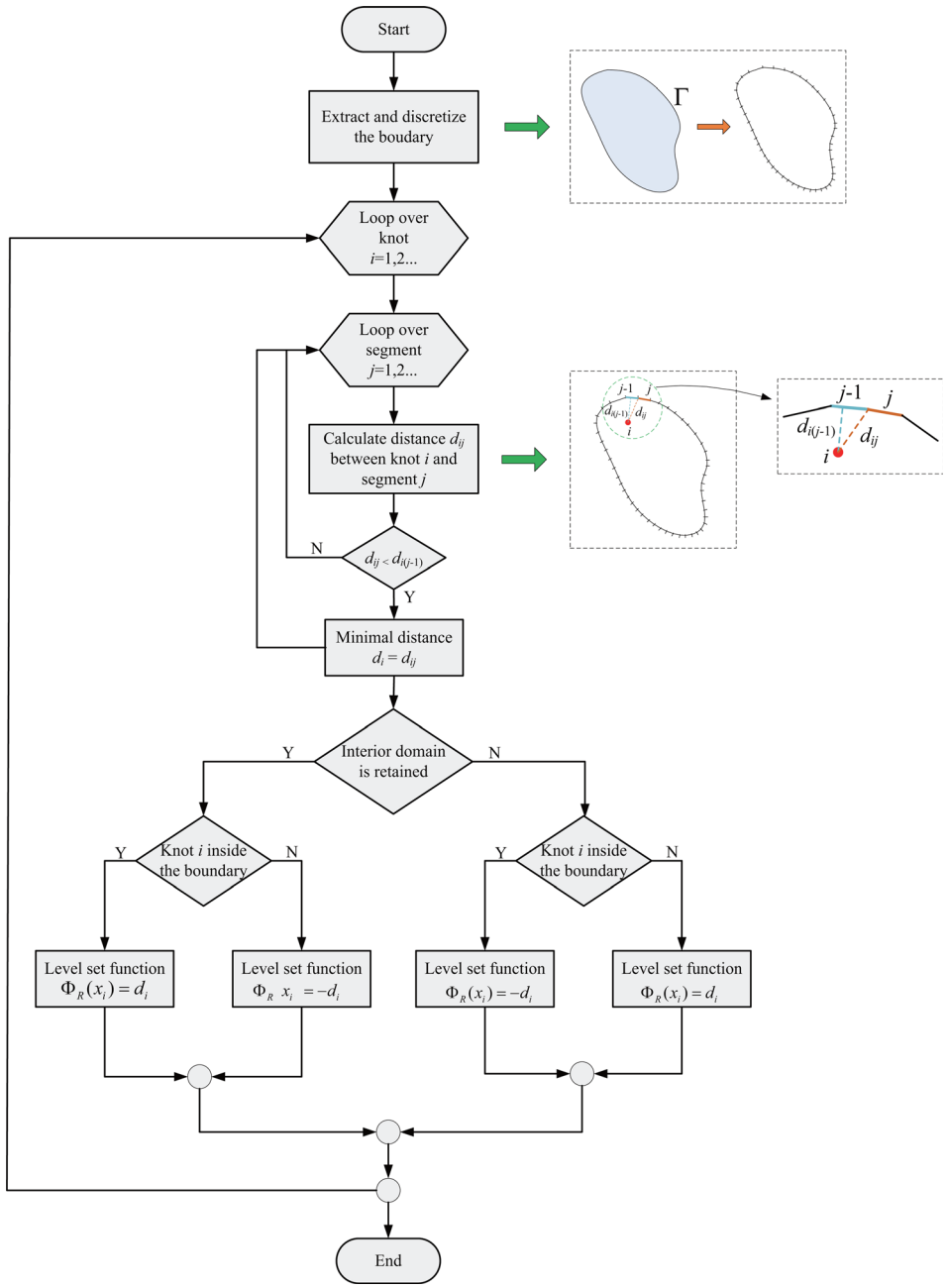

Fig. 4 Flowchart of contour function construction

- Step 3: Calculate the absolute value of level set function at knot i as $|\Phi_R(\mathbf{x}_i)| = d_i = \min(d_{ij}), j = 1, 2, \ldots m$.
- Step 4: Judge the position relation between knot i and boundary line Γ using ray casting algorithm.
- Step 5: If the interior domain of the model is retained while the exterior domain is cut off, the level set function is shown as follows:

$$\begin{cases} \Phi_R(\mathbf{x}_i) = d_i & (\text{knot } i \text{ is inside } \Gamma) \\ \Phi_R(\mathbf{x}_i) = -d_i & (\text{knot } i \text{ is outside } \Gamma) \end{cases} \tag{13}$$

If the interior domain of the model is cut off while the exterior domain is retained, the level set function is shown as follows:

$$\begin{cases} \Phi_R(\mathbf{x}_i) = -d_i & (\text{knot } i \text{ is inside } \Gamma) \\ \Phi_R(\mathbf{x}_i) = d_i & (\text{knot } i \text{ is outside } \Gamma) \end{cases} \tag{14}$$

Figure 4 concisely presents the flowchart of the above procedure. In total, a composite level set function can be setup by using R-function such as

$$\Phi(\mathbf{x}, t) = R(\Phi_F, \Phi_R^1, \Phi_R^2 \cdots \Phi_R^k) \tag{15}$$

where R denotes the R-function Boolean operations, Φ_F denotes free boundary level set function, and k denotes number of contour level set functions Φ_R^i for geometric constraints. Note that the choice of the level set function requires Lipschitz continuity [51]. It can be proved that contour function Φ_R is Lipschitz continuous by triangle inequality theorem (see the Appendix).

In the topology optimization of the prosthesis, the impenetrable constraint requires reservation of a region with finite thickness d along the profile of femur. Since that contour function Φ_R denotes the point-boundary distance, the level set of boundary domain can be represented by $0 \le \Phi_R \le d$. For each optimization iteration, we

keep the boundary domain by setting the expansion coefficients inside positive.

2.3 Definition and Analysis of Topology Optimization Problem. Generally, LSM topology optimization for minimum compliance design problem can be mathematically written in terms of the energy functional theory as follows:

$$\begin{aligned} &\text{Minimize}: J(\mathbf{u},\Phi) = \frac{1}{2}\int_D \left[E_{ijkl}\varepsilon_{ij}^{\mathrm{T}}(\mathbf{u})\varepsilon_{kl}(\mathbf{u})\right]H(\Phi)d\Omega \\ &\text{Subject to}: a(\mathbf{u},\mathbf{v},\Phi) = l(\mathbf{v},\Phi), \forall \mathbf{v}\in U, \mathbf{u}|_{\partial\Omega} = \mathbf{u}_0 \\ &\alpha_{i,\min} \le \alpha_i \le \alpha_{i,\max} \\ &V(\Omega) = \textstyle\int_D H(\Phi)d\Omega - V_{\max} \le 0 \end{aligned} \tag{16}$$

where $J(\mathbf{u}, \Phi)$ is the objective function, E_{ijkl} is the elastic modulus tensor, $\mathbf{u}_0$ is the prescribed displacement on the admissible Dirichlet boundary, and the inequality $V(\Omega) \le V_{\max}$ represents the volume constraint. α_i are the design variables, and $H(\Phi)$ is the Heaviside function of level set function Φ.

The energy bilinear form $a(\mathbf{u}, \mathbf{v}, \Phi)$ and the load linear form $l(\mathbf{v}, \Phi)$ of the state equation may be written in the weak variational forms as

$$a(\mathbf{u},\mathbf{v},\Phi) = \int_D E_{ijkl}\varepsilon_{ij}^{\mathrm{T}}(\mathbf{u})\varepsilon_{kl}(\mathbf{v})H(\Phi)d\Omega \tag{17}$$

$$l(\mathbf{v},\Phi) = \int_D \mathbf{f}\mathbf{v}H(\Phi)d\Omega + \int_\Gamma \mathbf{p}\mathbf{v}d\Gamma \tag{18}$$

where D is the design domain and Γ is its boundary, and $\mathbf{f}$ is the body force and $\mathbf{p}$ is the boundary traction. The original constrained optimization problem is converted into an unconstrained problem by the Lagrangian method [52] as

$$L(\mathbf{u},\Phi) = J(\mathbf{u},\Phi) + \Lambda\left[\int_D H(\Phi)d\Omega - V_{\max}\right] \tag{19}$$

In the conventional LSM, the steepest descent method is used to ensure the decrease of the objective function by setting the normal velocity ν_n to be the sensitivity of the objective function $J(\mathbf{u}, \Phi)$ with respect to the boundary variation of the design [27]. However, in the parameterization LSM, the normal velocity field ν_n in Eq. (7) is substituted into Eq. (19) to express the Lagrangian function as

$$\frac{\partial L(\mathbf{u},\Phi)}{\partial t} = \sum_{i=1}^{n}\frac{\partial J(\mathbf{u},\Phi)}{\partial \alpha_i(t)}\frac{\partial \alpha_i(t)}{\partial t} + \Lambda\sum_{i=1}^{n}\frac{\partial V(\mathbf{u},\Phi)}{\partial \alpha_i(t)}\frac{\partial \alpha_i(t)}{\partial t} \tag{20}$$

Since the partial derivative of Heaviside function $H(\Phi)$ is Dirac function $\delta(\Phi)$ and $d\Gamma = \delta(\Phi)|\nabla\Phi|d\Omega$ [27], the design sensitivities may be expressed as

$$\frac{\partial J(\mathbf{u},\Phi)}{\partial \alpha_i(t)} = -\frac{1}{2}\int_D \left[E_{ijkl}\varepsilon_{ij}^{\mathrm{T}}(\mathbf{u})\varepsilon_{kl}(\mathbf{u})\right]\phi_i\delta(\Phi)d\Omega \tag{21}$$

$$\frac{\partial V(\mathbf{u},\Phi)}{\partial \alpha_i(t)} = \int_D \phi_i\delta(\Phi)d\Omega \tag{22}$$

where $\delta(\Phi)$ is defined as $(1/\pi)(\xi/\Phi^2 + \xi^2)$ and ξ is chosen as 2–4 times the mesh size, α_i is the expansion coefficients, i.e., design variables, and $i = 1, 2, \ldots, n$, where n is the number of CS-RBF knots. The sensitivity analysis is performed to update the design variables. More details of the sensitivity analysis are discussed in Refs. [36,37].

In the conventional LSM topology optimization, the "ersatz material" approach [27,29] is utilized to the finite element analysis, where a weak material is adopted to avoid singularity and the element stiffness is proportional to the area portion of the solid material within the element. However, this method is not accurate enough, especially when the element size is large. In order to improve the accuracy, Wei et al. [38] applied the XFEM to the LSM topology optimization and the numerical examples showed that the XFEM led to more accurate results.

Using the four-node rectangular element on a fixed Eulerian grid as an example, the "ersatz material" method is used to evaluate the element stiffness matrix in solid and void elements. The solid material part of the boundary-crossing element is divided into subtriangles, and the stiffness matrix of the element is expressed as

$$\mathbf{K_E} = \mathbf{K_s} + \mathbf{K_w} = \int_{\Omega_s}\mathbf{B}^{\mathrm{T}}\mathbf{D}_s\mathbf{B}d\Omega + \int_{\Omega_w}\mathbf{B}^{\mathrm{T}}\mathbf{D}_w\mathbf{B}d\Omega \tag{23}$$

where $\mathbf{D}_s$ and $\mathbf{D}_w$ are the elastic matrices of the solid material and weak material components, and $\mathbf{B}$ is the displacement differentiation matrix for the whole element. The highly efficient Hammer quadrature method [44,53] is applied to evaluate the solid material stiffness matrix.

3 Results of Total Femur Prosthesis

In this section, the example shows the optimized total femur prostheses targeting at different weights in the context of structural minimum compliance design.

Figure 5 shows a typical scaled femur fitted into the rectangular design domain in yellow, whose width is normalized to 1. Note that the envelope of the artificial femur for optimization is originated from RhinoSurf, a sample library of commercial CAD software Rhino [54]. The width and height of the design domain are 1 and 4.78, respectively. According to the impenetrable boundary constraint of the artificial femur, we set the fixed region with constant shell thickness of 0.056. Therefore, optimization can be only implemented inside the cavity enclosed by the femur shell, and the background domain in Fig. 5 will be completely cut out. To control the weight of the artificial femur, three designated cavity fill ratios 34%, 54%, and 74% corresponding to volume ratio (the ratio of the total shaded area to the rectangular area of the design domain) 15%, 20%, and 25% are considered. Uniform traction is applied on the right hand side of rectangular design domain, which effectively transmits the pressure on the proximal femur structure. The constraints of all degrees-of-freedom at the left hand side of the design domain are equivalent to fixation of the distal femur. The material parameters are given as follows: Young's modulus for solid material phase is 1000, for weak phase is 1, and Poisson's ratio for the both phases is 0.3. (Since the prosthesis is made of one isotropic material, it actually does not matter what Young's modulus is used for the solid phase. The Poisson's ratio of titanium alloy is assumed to be 0.3.) The design domain is discretized with a mesh of 80×320 quadrilateral elements.

By using the contour function method, the profile of the femur can be imposed as zero level set. The level set function has positive values inside the femur and negative values outside when Eq. (13) is applied. Optimization process of the case with 20% volume ratio is shown in Fig. 6, and the corresponding convergent

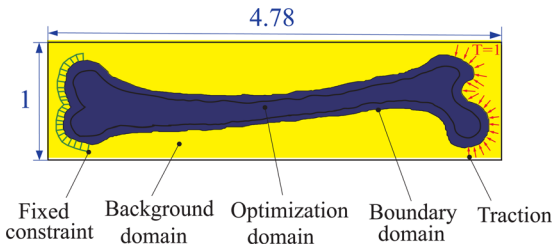

Fig. 5 Design domain of the femur model

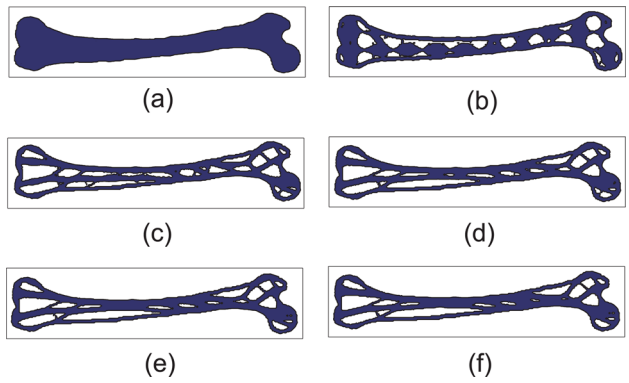

Fig. 6 Optimization stages of the femur with volume ratio 20%: (*a*) Initial design, (*b*) step 2, (*c*) step 6, (*d*) step 12, (*e*) step 16, and (*f*) step 20 (final result)

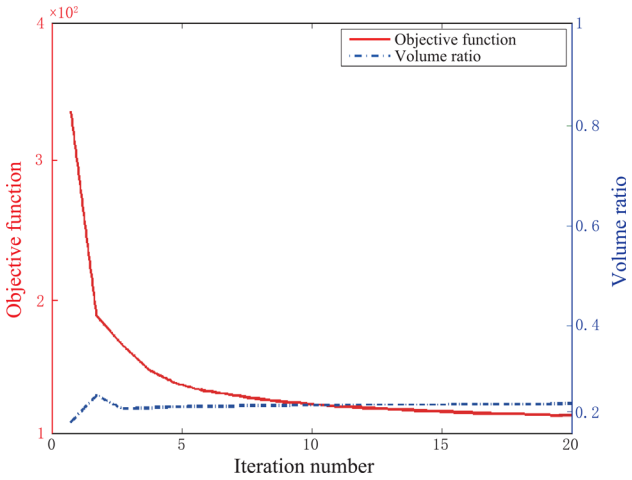

Fig. 7 Convergent histories of the femur optimization

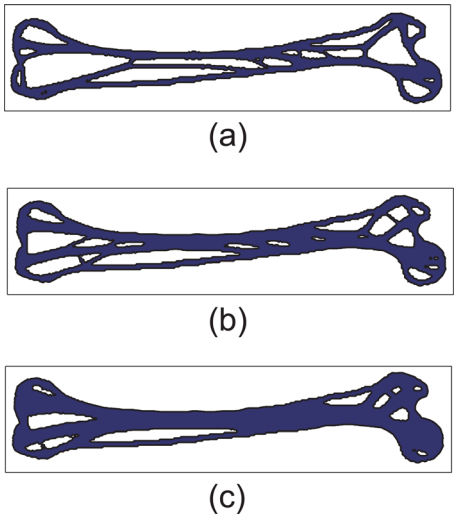

Fig. 8 Optimized femur results of different volume ratios: (*a*) 0.15, (*b*) 0.2, and (*c*) 0.25

histories are given in Fig. 7. The optimized results of a series of different volume ratios are illustrated in Fig. 8. The total strain energy, calculated by the integration of the total energy density over the whole design domain, of the optimized femur designs with volume ratio 15%, 20%, and 25% are 1.88×10^2, 1.34×10^2, and 1.208×10^2, respectively.

The limitations of the method are discussed as follows. First, our method only allows macroscopic change of the structural topology for homogenized materials. Khanoki and Pasini [7] designed a cellular material with spatially periodic lattice microstructure for implants using porous tantalum, a biocompatible material. The controllable microstructure, e.g., material porosity, can be optimized with a fixed structural geometry. In the future, a better design can be achieved by optimization based on multiscale analysis. Another limitation is that the impact of the high-cycle loading is ignored in current static analysis. Fatigue analysis of the femur prosthesis should be involved in future researches [5,6]. Further study is also necessary to extend the optimization of femur to 3D topology for the realistic designs. Finally, quantitative measurement of both bone resorption [55,56] and implant stability [57–59] should be performed to assess both the short and long term performances of the implant.

4 Discussions

There has been a substantial increase of femur replacement used as a limb-saving option in the occasion of bone tumor treatment and other nononcologic indications. One major problem is how to design an efficient prosthesis in the sense: (a) match the contact with the articular cartilage to avoid wear and erosion; (b) maximal stiffness subject to the target total weight. In this paper, we present a parameterized LSM topology optimization with arbitrary geometric constraints on the femur prosthesis design. In contrast to the conventional methods that represent the geometry explicitly and may result in the zigzag pattern, smooth geometry of the structure, which is implicitly represented by the level set function, will be obtained in current method. The concave profile of the original femur is preserved with a finite thickness by applying geometric constraints based on the contour function method, while the topology optimization is only carried out inside the cavity.

The key concept of the contour method is to construct Lipschitz continuous contour function, which can easily represent arbitrary geometries by setting the boundary as the zero level set and directly assigning the signed minimal point-boundary distances to the level set function. The geometric constraints are unified to the free boundary level set function by using the R-functions into the expansion coefficients. A numerical example of total femur prosthesis illustrates the effectiveness and stability of the method. The results show that the optimized structures have sufficient smoothness to satisfy the design requirement.

Due to the complex internal geometry generated by the topology optimization, it is very difficult to manufacture the structure by traditional subtractive machining. The use of 3D printing technology even allows the designers to gain the power to control over the topology of microstructure [60,61]. In the future, we will extend the optimization capability to the 3D problems, and further integrate the implicit representation of the complex geometry by the level set function with the 3D printing technology [62] to expand the practical applications of the topology optimization.

Acknowledgment

This research has been supported by the National Natural Science Foundation of China (51475180 and 51275182), and also sponsored in part by the National Key Technology R&D Program of China (Grant No. 2013ZX04005-011) and the East Lake High-tech Zone Science and Technology Innovation Project (Grant No. 20130101017).

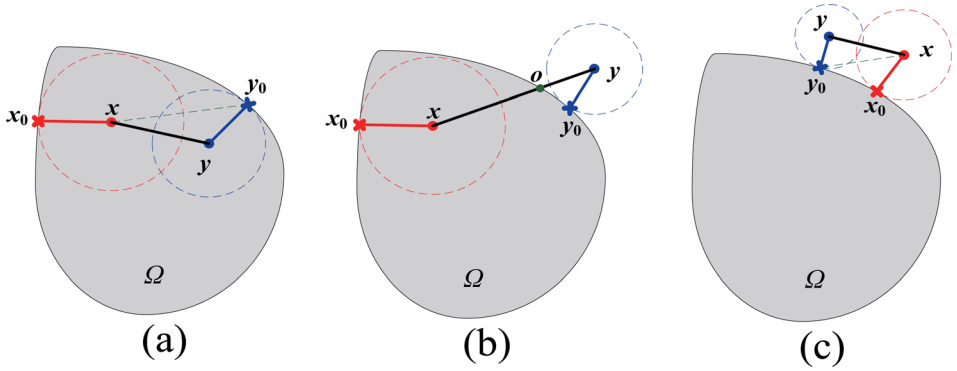

Fig. 9 Point-domain position relationship for two arbitrary points: (*a*) Both are inside the domain, (*b*) one is inside and the other is outside the domain, and (*c*) both are outside the domain

Appendix: Lipschitz Continuity of the Contour Function

Recalling that the level set function Φ should satisfy Lipschitz continuity [51] defined as

$$|\Phi(\mathbf{x}) - \Phi(\mathbf{y})| \le K|\mathbf{x} - \mathbf{y}| \tag{A1}$$

Thus, the contour function Eqs. (13) and (14) have to satisfy the above equation. According to point-domain position, two arbitrary points $\mathbf{x}$ and $\mathbf{y}$ and a domain Ω can be classified into three cases: (1) both inside the domain (Fig. 9(*a*)), (2) one inside and the other outside the domain (Fig. 9(*b*)), and (3) both outside the domain (Fig. 9(*c*)). In Fig. 9, suppose that the boundary of domain Ω is the zero level set, the minimal point-boundary distances of $\mathbf{x}$ and $\mathbf{y}$ are $\overline{\mathbf{x}\mathbf{x}_0}$ and $\overline{\mathbf{y}\mathbf{y}_0}$, respectively. Assuming $\overline{\mathbf{x}\mathbf{x}_0} > \overline{\mathbf{y}\mathbf{y}_0}$, the continuity proof is given below.

If $\mathbf{x}$ and $\mathbf{y}$ are both inside or outside Ω (Fig. 9(*a*) or 9(*c*)), according to the relationship of triangle sides, we can obtain

$$\overline{\mathbf{x}\mathbf{y}_0} - \overline{\mathbf{y}\mathbf{y}_0} \le \overline{\mathbf{x}\mathbf{y}} \tag{A2}$$

Due to

$$\overline{\mathbf{x}\mathbf{x}_0} \le \overline{\mathbf{x}\mathbf{y}_0} \tag{A3}$$

Lipschitz continuity can be easily proved as

$$|\Phi(\mathbf{x}) - \Phi(\mathbf{y})| = |\overline{\mathbf{x}\mathbf{x}_0} - \overline{\mathbf{y}\mathbf{y}_0}| \le \overline{\mathbf{x}\mathbf{y}} \tag{A4}$$

If $\mathbf{x}$ is inside Ω and $\mathbf{y}$ is outside Ω (Fig. 9(*b*)), assuming point $\mathbf{o}$ is the intersection point of $\overline{\mathbf{x}\mathbf{y}}$ and the boundary, we can obtain the following inequalities:

$$\overline{\mathbf{x}\mathbf{x}_0} \le \overline{\mathbf{x}\mathbf{o}} \tag{A5}$$

$$\overline{\mathbf{y}\mathbf{y}_0} \le \overline{\mathbf{y}\mathbf{o}} \tag{A6}$$

Lipschitz continuity can be proved as

$$|\Phi(\mathbf{x}) - \Phi(\mathbf{y})| = |\overline{\mathbf{x}\mathbf{x}_0} + \overline{\mathbf{y}\mathbf{y}_0}| \le |\overline{\mathbf{x}\mathbf{o}} + \overline{\mathbf{y}\mathbf{o}}| = \overline{\mathbf{x}\mathbf{y}} \tag{A7}$$

References

[1] Bickels, J., Malawer, M. M., Meller, I., Kollender, Y., Rubert, K. M., and Henshaw, R. M., 1999, "Proximal and Total Femur Resections With Endoprosthetic Reconstruction," 10th International Symposium of the International Society of Limb Salvage (ISOLS).

[2] Hoell, S., Butschek, S., Gosheger, G., Dedy, N., Dieckmann, R., Henrichs, M., Daniilidis, K., and Hardes, J., 2011, "Intramedullary and Total Femur Replacement in Revision Arthroplasty as a Last Limb-Saving Option: Is There Any Benefit From the Less Invasive Intramedullary Replacement?," J. Bone Jt. Surg. Br., **93-B**(11), pp. 1545–1549.

[3] Sumner, D. R., and Galante, J. O., 1992, "Determinants of Stress Shielding: Design Versus Materials Versus Interface," Clin. Orthop. Relat. Res., **274**, pp. 79–96.

[4] Donati, D., Zavatta, M., Gozzi, E., Giacomini, S., Campanacci, L., and Mercuri, M., 2001, "Modular Prosthetic Replacement of the Proximal Femur After Resection of a Bone Tumour: A Long-Term Follow-Up," J. Bone Jt. Surg., **83-B**, pp. 1156–1160.

[5] Khanoki, S. A., and Pasini, D., 2013, "Fatigue Design of a Mechanically Biocompatible Lattice for a Proof-of-Concept Femoral Stem," J. Mech. Behav. Biomed. Mater., **22**, pp. 65–83.

[6] Khanoki, S. A., and Pasini, D., 2013, "The Fatigue Design of a Bone Preserving Hip Implant With Functionally Graded Cellular Material," ASME J. Med. Devices., **7**(2), p. 020907.

[7] Khanoki, S. A., and Pasini, D., 2012, "Multiscale Design and Multiobjective Optimization of Orthopedic Hip Implants With Functionally Graded Cellular Material," ASME J. Biomech. Eng., **134**(3), p. 031004.

[8] Zhu, X. H., He, G., and Gao, B. Z., 2005, "The Application of Topology Optimization on the Quantitative Description of the External Shape of Bone Structure," J. Biomech., **38**, pp. 1612–1620.

[9] Nowak, M., 2006, "Structural Optimization System Based on Trabecular Bone Surface Adaptation," Struct. Multidiscip. Optim., **32**(3), pp. 241–249.

[10] Bagge, M., 2000, "A Model of Bone Adaptation as an Optimization Process," J. of Biomech., **33**(11), pp. 1349–1357.

[11] Sutradhar, A., Paulino, G. H., Miller, M. J., and Nguyen, T. H., 2010, "Topological Optimization for Designing Patient-Specific Large Craniofacial Segmental Bone Replacements," Proc. Natl. Acad. Sci., **107**(30), pp. 13222–13227.

[12] Nicolella, D. P., Thacker, B. H., Katoozian, H., and Davy, D. T., 2006, "The Effect of Three-Dimensional Shape Optimization on the Probabilistic Response of a Cemented Femoral Hip Prosthesis," J. Biomech., **39**(7), pp. 1265–1278.

[13] Li, G. Y., Xu, F., Huang, X. X. D., and Sun, G. Y., 2014, "Topology Optimization of an Automotive Tailor-Welded Blank (TWB) Door," ASME J. Mech. Des., **137**(5), p. 055001.

[14] Yamada, T., Izui, K., and Nishiwaki, S., 2011, "A Level Set-Based Topology Optimization Method for Maximizing Thermal Diffusivity in Problems Including Design-Dependent Effects," ASME J. Mech. Des., **133**(3), p. 031011.

[15] Michell, A., 1904, "The Limits of Economy of Material in Frame Structures," Philos. Mag., **8**(47), pp. 589–597.

[16] Bendsøe, M. P., and Kikuchi, N., 1988, "Generating Optimal Topologies in Structural Design Using a Homogenization Method," CMAME, **71**(2), pp. 197–224.

[17] Bendsøe, M. P., 1989, "Optimal Shape Design as a Material Distribution Problem," Struct. Optim., **1**(4), pp. 193–202.

[18] Xie, Y. M., and Steven, G. P., 1993, "A Simple Evolutionary Procedure for Structural Optimization," Comput. Struct., **49**(5), pp. 885–896.

[19] Nishiwaki, S., Frecker, M. I., Min, S., and Kikuchi, N., 1998, "Topology Optimization of Compliant Mechanisms Using the Homogenization Method," Int. J. Numer. Methods Eng., **42**(3), pp. 535–559.

[20] Sigmund, O., 2001, "A 99 Line Topology Optimization Code Written in MATLAB," Struct. Multidiscip. Optim., **21**(2), pp. 120–127.

[21] Reynolds, D., McConnachie, J., Bettess, P., Christie, W. C., and Bull, J. W., 1999, "Reverse Adaptivity—A New Evolutionary Tool for Structural Optimization," Int. J. Numer. Methods Eng., **45**(5), pp. 529–552.

[22] Wang, M. Y., and Wang, X. M., 2004, "PDE-Driven Level Sets, Shape Sensitivity and Curvature Flow for Structural Topology Optimization," Comput. Model. Eng. Sci., **6**(4), pp. 373–396.

[23] Bendsøe, M., and Sigmund, O., 2003, *Topology Optimization: Theory, Methods and Applications*, Springer, Berlin.

[24] Osher, S., and Sethian, J. A., 1988, "Fronts Propagating With Curvature-Dependent Speed: Algorithms Based on Hamilton–Jacobi Formulations," J. Comput. Phys., **79**(1), pp. 12–49.

[25] Sethian, J. A., and Wiegmann, A., 2000, "Structural Boundary Design Via Level Set and Immersed Interface Methods," J. Comput. Phys., **163**(2), pp. 489–528.
[26] Osher, S. J., and Santosa, F., 2001, "Level Set Methods for Optimization Problems Involving Geometry and Constraints: I. Frequencies of a Two-Density Inhomogeneous Drum," J. Comput. Phys., **171**(1), pp. 272–288.
[27] Wang, M. Y., Wang, X. M., and Guo, D., 2003, "A Level Set Method for Structural Topology Optimization," Comput. Methods Appl. Mech. Eng., **192**(1), pp. 227–246.
[28] Allaire, G., Jouve, F., and Toader, A., 2002, "A Level-Set Method for Shape Optimization," C. R. Math., **334**(12), pp. 1125–1130.
[29] Allaire, G., Jouve, F., and Toader, A., 2004, "Structural Optimization Using Sensitivity Analysis and a Level-Set Method," J. Comput. Phys., **194**(1), pp. 363–393.
[30] Allaire, G., Gournay, F. D., Jouve, F., and Toader, A., 2005, "Structural Optimization Using Topological and Shape Sensitivity Via a Level Set Method," Control Cybern., **34**, pp. 59–80.
[31] Zhu, B. L., Zhang, X. M., and Fatikow, S., 2014, "A Velocity Predictor-Corrector Scheme in Level Set-Based Topology Optimization to Improve Computational Efficiency," ASME J. Mech. Des., **136**(9), p. 091001.
[32] Zhu, B. L., Zhang, X. M., and Fatikow, S., 2014, "Level Set-Based Topology Optimization of Hinge-Free Compliant Mechanisms Using a Two-Step Elastic Modeling Method," ASME J. Mech. Des., **136**(3), p. 031007.
[33] Wang, S. Y., and Wang, M. Y., 2006, "Radial Basis Functions and Level Set Method for Structural Topology Optimization," Int. J. Numer. Methods Eng., **65**(12), pp. 2060–2090.
[34] Wang, S. Y., Lim, K. M., Khoo, B. C., and Wang, M. Y., 2007, "An Extended Level Set Method for Shape and Topology Optimization," J. Comput. Phys., **221**(1), pp. 395–421.
[35] Luo, Z., Tong, L. Y., Wang, M. Y., and Wang, S. Y., 2007, "Shape and Topology Optimization of Compliant Mechanisms Using a Parameterization Level Set Method," J. Comput. Phys., **227**(1), pp. 680–705.
[36] Luo, Z., Wang, M. Y., Wang, S. Y., and Wei, P., 2008, "A Level Set-Based Parameterization Method for Structural Shape and Topology Optimization," Int. J. Numer. Methods Eng., **76**(1), pp. 1–26.
[37] Luo, Z., Tong, L. Y., and Kang, Z., 2009, "A Level Set Method for Structural Shape and Topology Optimization Using Radial Basis Functions," Comput. Struct., **87**(7), pp. 425–434.
[38] Wei, P., Wang, M. Y., and Xing, X. H., 2010, "A Study on X-Fem in Continuum Structural Optimization Using a Level Set Model," Comput.-Aided Des., **42**(8), pp. 708–719.
[39] Chen, J., Shapiro, V., Suresh, K., and Tsukanov, I., 2007, "Shape Optimization With Topological Changes and Parametric Control," Int. J. Numer. Methods Eng., **71**(3), pp. 313–346.
[40] Chen, J., Freytag, M., and Shapiro, V., 2008, "Shape Sensitivity of Constructively Represented Geometric Models," Comput. Aided Geom. Des., **25**(7), pp. 470–488.
[41] Chen, S., Wang, M. Y., and Liu, A. Q., 2008, "Shape Feature Control in Structural Topology Optimization," Comput.-Aided Des., **40**(9), pp. 951–962.
[42] Guo, X., Zhang, W., and Zhong, W., 2014, "Explicit Feature Control in Structural Topology Optimization Via Level Set Method," Comput. Methods Appl. Mech. Eng., **272**, pp. 354–378.
[43] Allaire, G., Jouve, F., and Michailidis, G., 2014, "Thickness Control in Structural Optimization Via a Level Set Method," https://hal.archives-ouvertes.fr/hal-00985000
[44] Liu, T., Wang, S. T., Li, B., and Gao, L., 2014, "A Level-Set-Based Topology and Shape Optimization Method for Continuum Structure Under Geometric Constraints," Struct. Multidiscip. Optim., **50**(2), pp. 253–273.
[45] Liu, T., Li, B., Wang, S. T., and Gao, L., 2014, "Eigenvalue Topology Optimization of Structures Using a Parameterized Level Set Method," Struct. Multidiscip. Optim., **50**(4), pp. 573–591.
[46] Wang, B., and Cheng, G., 2006, "Design of Cellular Structure for Optimum Efficiency of Heat Dissipation," IUTAM Symposium on Topological Design Optimization of Structures, Machines and Materials, Springer, Berlin, pp. 107–116.
[47] Wendland, H., 1995, "Piecewise Polynomial, Positive Definite and Compactly Supported Radial Functions of Minimal Degree," Adv. Comput. Math., **4**(1), pp. 389–396.
[48] Schaback, R., and Wendland, H., 2001, "Characterization and Construction of Radial Basis Functions," *Multivar. Approximation Appl.*, N. Dyn, D. Leviatan, D. Levin, and A. Pinkus, eds., Cambridge University Press, Cambridge, UK, pp. 1–24.
[49] Hales, T. C., 2007, "The Jordan Curve Theorem, Formally and Informally," Am. Math. Mon., **114**(10), pp. 882–894.
[50] Shimrat, M., 1962. "Algorithm 112: Position of Point Relative to Polygon," Commun. ACM, **5**, pp. 446–451.
[51] O'Searcoid, M., 2006, *Metric Spaces*, Springer, Berlin.
[52] Wang, S., and Wang, M. Y., 2006, "Radial Basis Functions and Level Set Method for Structural Topology Optimization," Int. J. Numer. Methods Eng., **65**(12), pp. 2060–2090.
[53] Dunavant, D. A., 1985, "High Degree Efficient Symmetrical Gaussian Quadrature Rules for the Triangle," Int. J. Numer. Methods Eng., **21**(6), pp. 1129–1148.
[54] 2014, "RESURF," http://www.resurf3d.com
[55] Glassman, A., Bobyn, J., and Tanzer, M., 2006, "New Femoral Designs: Do They Influence Stress Shielding?," Clin. Orthop. Relat. Res., **453**, pp. 64–74.
[56] Huiskes, R., Weinans, H., and Van Rietbergen, B., 1992, "The Relationship Between Stress Shielding and Bone Resorption Around Total Hip Stems and the Effects of Flexible Materials," Clin. Orthop. Relat. Res., **274**, pp. 124–134.
[57] Abdul-Kadir, M. R., Hansen, U., Klabunde, R., Lucas, D., and Amis, A., 2008, "Finite Element Modelling of Primary Hip Stem Stability: The Effect of Interference Fit," J. Biomech., **41**(3), pp. 587–594.
[58] Viceconti, M., Brusi, G., Pancanti, A., and Cristofolini, L., 2006, "Primary Stability of an Anatomical Cementless Hip Stem: A Statistical Analysis," J. Biomech., **39**(7), pp. 1169–1179.
[59] Viceconti, M., Monti, L., Muccini, R., Bernakiewicz, M., and Toni, A., 2001, "Even a Thin Layer of Soft Tissue May Compromise the Primary Stability of Cementless Hip Stems," Clin. Biomech., **16**(9), pp. 765–775.
[60] Benvenuti, S., Ceccanti, F., and De Kestelier, X., 2013, "Living on the Moon: Topological Optimization of a 3D-Printed Lunar Shelter," NEXUS Network J., **15**(2), pp. 285–302.
[61] Snelling, D., Li, Q., Meisel, N., Williams, C. B., Batra, R. C., and Druschitz, A. P., 2015, "Lightweight Metal Cellular Structures Fabricated Via 3D Printing of Sand Cast Molds," Adv. Eng. Mater., **17**(7), pp. 923–932.
[62] Gerstle, T. L., Ibrahim, A. M. S., Kim, P. S., Lee, B. T., and Lin, S. J., 2014, "A Plastic Surgery Application in Evolution: Three-Dimensional Printing," Plast. Reconstr. Surg., **133**(2), pp. 446–451.